Geophysical Research Letters

Supporting Information for

Enhanced Trans-seasonal ENSO Impact on East Asian-Western Pacific Climate in Warmer Future: An Emergent Constraint from multi-Large Ensembles

Lu Wang[1], Xiaolong Chen[2*], Yan Zhao[1], Tianjun Zhou[2,3], Lin Chen[1], Ming Sun[1,4]

1 State Key Laboratory of Climate System Prediction and Risk Management/Key Laboratory of Meteorological Disaster, Ministry of Education/Collaborative Innovation Center on Forecast and Evaluation of Meteorological Disasters, Nanjing University of Information Science and Technology, Nanjing, China.

2 State Key Laboratory of Earth System Numerical Modeling and Application, Institute of Atmospheric Physics, Chinese Academy of Sciences, Beijing, China

3 University of Chinese Academy of Sciences, Beijing, China

4 Anhui Climate Center, Anhui Meteorological Service, Hefei, China

*Corresponding author: Xiaolong Chen (chenxiaolong@mail.iap.ac.cn)

Contents of this file

Table S1
Texts S1 to S4
Figures S1 to S6

Introduction

This Supporting Information contains 1 table, 4 texts, and 6 figures.

Table S1 lists basic information of 3 CMIP5 and 5 CMIP6 Single Model Initial-condition Large Ensembles (SMILEs) used in this study, including model names, affiliated institutions and locations, member numbers, experiments.

Texts S1 to S4 describe model and reanalysis data (Text S1), WNPAC definition and ENSO classification (Text S2), hierarchical statistical framework for multi-step emergent constraint (Text S3), and validating robustness of ENSO-WNPAC relationship definition (Text S4), respectively.

Figure S1 shows model uncertainty of ENSO-WNPAC relationship changes related to different ENSO decaying regimes. It is used to validate the reconstruction methods and display the relative contributions of different properties associated with ENSO decaying regimes to the model uncertainty in the projected changes of ENSO-WNPAC correlation coefficient ($\Delta C_{E\text{-}W}$).

Figure S2 shows diverse patterns of correlation coefficient between D(-1)JF Nino3.4 index and JJA 850-hPa vorticity and winds during the historical period (1965-2005) in 8 SMILEs.

Figure S3 shows the same as Figure S2, but for the future period (2050-2099) under RCP8.5/SSP5-8.5 scenario.

Figure S4 shows the same as Figure S2, but for difference between the future (Figure S3) and historical periods (Figure S2).

Figures S2-S4 are used to define a model-specific ENSO-WNPAC correlation depending on the pattern in each model and compare with that defined in a conventional fixed region in the main text (Figure 1a). It shows consistent result of change in ENSO-WNPAC relationship in each model, no matter which definition method is employed.

Figure S5 shows physical mechanism of model spread in historical D(-1)JF ENSO intensity (slow-decay regime) impacting on future change of ENSO-related JJA anomalies over the WNP.

Figure S6 shows the trans-seasonal ENSO-WNPAC correlation coefficient ($C_{E\text{-}W}$) of SSP2-4.5 versus SSP5-8.5 during 2050-2099 in three CMIP6 SMILEs. Considering the influence of internal variability, the $C_{E\text{-}W}$ are rather consistent in high and middle emission scenarios, indicating the emergent constraints proposed in this study could also be valid in lower emission scenario.

Table S1. Basic information of 3 CMIP5 and 5 CMIP6 SMILEs used in this study.

No.	Model	Institute/Location	Member	Experiment
1	CanESM2	CCCma/Canada	50	CMIP5 (historical, rcp85)
2	CESM1	NCAR/USA	42	CMIP5 (historical, rcp85)
3	MPI-GE	MPI/Germany	100	CMIP5 (historical, rcp85)
4	CanESM5	CCCma/Canada	50	CMIP6 (historical, ssp585)
5	CESM2	NCAR/USA	100	CMIP6 (historical, ssp585)
6	FGOALS-g3	IAP/China	108	CMIP6 (historical, ssp585)
7	MIROC6	MIROC/Japan	50	CMIP6 (historical, ssp585)
8	MPI-ESM1-2-LR	MPI/Germany	50	CMIP6 (historical, ssp585)

Text S1. Model and reanalysis data

The SMILEs under historical forcing (i.e., historical simulations) and the high greenhouse-gas emission scenarios (i.e., Shared Socioeconomic Pathways 5-8.5 for CMIP6 or Representative Concentration Pathways 8.5 for CMIP5) (Taylor et al., 2012; Eyring et al., 2016) generated by 8 climate models are used in our analysis (Table S1). The radiative forcings under SSP5-8.5 from CMIP6 and RCP8.5 from CMIP5 both increase to around 8.5 W m^{-2} in 2100, although the details in emission pathways of individual forcings are not identical (O'Neil et al., 2016). To obtain robust forced signals of interannual variability related to ENSO, we need enough large member numbers in each model ensemble (Z. Zhou et al., 2024). Thus, models were selected based on the availability of at least 40-initial condition ensemble members, with CESM2 (Rodgers et al., 2021), FGOALS-g3 (Lin et al., 2022) and MPI-GE (Maher et al., 2019) providing more than 100 ensemble members, which are referred to as super-SMILEs. Given the extensive use of the SMILE generated by CESM1 in previous studies, its results, containing 42 members, are also included in this study. To examine the dependence on emission scenario, 3 available SMILEs under SSP2-4.5 from CMIP6, that is CanESM5 (50 members), MIROC6 (50 members) and MPI-ESM1-2-LR (30 members), are additionally used to compare with the results under SSP5-8.5. The outputs of monthly mean SST, precipitation, and 850-hPa wind are employed for analysis, focusing on the projected changes during 2050-2099 relative to 1956-2005.

To illustrate the trans-seasonal impacts of pre-winter ENSO with different decaying pace on summer WNPAC in observation and constrain the projected ENSO-WNPAC relationship in future, SST, precipitation and 850-hPa wind from ECMWF Reanalysis v5 (ERA5) during 1950-2024 (Soci et al., 2024) are used. The ERA5 data, forced by observationally-based SST and sea ice, has the best performance on representing the East Asia climate (Kim & Lee, 2022) and the longest span extending to recent years.

Text S2. WNPAC definition and ENSO classification

The Nino3.4 index is D(-1)JF SST anomaly averaged over the domain (5°S-5°N, 170-120°W) and the WNPAC index is JJA 850-hPa vorticity anomaly averaged in the western North Pacific region (10-30°N, 110-160°E). Subsequently, the probability density function (PDF) of the correlation coefficient between the D(-1)JF Nino3.4 index and JJA WNPAC index ($C_{E\text{-}W}$) is constructed based on all members for each model under Gaussian hypothesis. The $C_{E\text{-}W}$ in the observation is negative since anomalous anticyclone usually following El Niño events and vice versa.

Since ENSO decaying pace substantially contributes to the projected uncertainty of WNPAC response (Chen et al., 2016; Wu et al., 2020, 2021), to distinguish the effects of different ENSO evolution on $C_{E\text{-}W}$ and understand the mechanisms of future change, we simply divide the ENSO events (that is D(-1)JF Niño 3.4 index anomalies large than 0.5℃ or less than -0.5℃) into two groups: fast-decay and slow-decay. In the fast-decay group, Nino 3.4 indexes in D(-1)JF and JJA have opposite sign, whereas the sign keep the same in the slow-decay group.

Text S3. Hierarchical statistical framework for multi-step emergent constraint

Following the previous studies (e.g. Bowman et al., 2018; Chen et al., 2020), the hierarchical statistical framework for emergent constraint is briefly described as follows. The linear relationship between constraining factor (X) and target to be constrained (Y) across models is expressed as

$$Y = \bar{Y} + r(X - \bar{X}); \quad (1)$$

in which the bar terms are multi-model mean, regression coefficient $r = (\sigma_Y/\sigma_X)\rho$, ρ the inter-model correlation coefficient between X and Y, σ the inter-model standard deviation. When implementing the constraint, r should be adjusted by dividing $(1+\mathrm{SNR}^{-1})$ in this additive-noise model under Gaussian assumptions, where signal-to-ratio of X, $\mathrm{SNR}=\sigma_X^2/\sigma_R^2$, and σ_R standard deviation of observational variable or that constrained in the previous step used to constrain Y in the current step. After each step, the mean and standard deviation of constrained Y (Y_C) is derived from

$$\overline{Y_C} = \bar{Y} + \frac{r}{1+\mathrm{SNR}^{-1}}(\overline{X_R} - \bar{X}); \quad (2)$$

$$\sigma_{Y_C}^2 = \left(1 - \frac{\rho^2}{1+\mathrm{SNR}^{-1}}\right)\sigma_Y^2. \quad (3)$$

Since model uncertainties in historical simulations could propagate into future projections through multiple processes, we develop a multi-step approach to correct key variables and reduce uncertainty associated with each process. A similar strategy has been successfully applied to reduce model spread in temperature projections over the Tibetan Plateau (Hu et al., 2024). In this study, we first constrain key components of the future change of ENSO-WNPAC relationship based on distinct mechanisms from slow-decay and fast-decay ENSO regimes individually, and finally constrain the total change by integrating the constrained key components.

Observational-based correlation coefficients between D(-1)JF Nino3.4 and JJA WNPAC index in fast-decay and slow-decay ENSO events, C_{FH} and C_{SH} ("H" in subscript means historical period), respectively, are the initial constraining factors in the multi-step emergent constraint method. Distributions of these two factors are derived from the 75-year ERA5 reanalysis by resampling without replacement. To be consistent with the length used in models, we randomly select 50 years from the 75-year data to calculate the corresponding C_{FH} and C_{SH}, and repeat it for 50 times. Then, the distributions of C_{FH} and C_{SH} are estimated based on the 50 samples under the Gaussian assumption.

Text S4. Validating robustness of ENSO-WNPAC relationship definition

Considering that the position of the ENSO-induced WNPAC pattern might differ among models, or potentially shift between future projections and historical simulations for a given model, the spatial patterns of the ENSO-WNPAC relationship for individual models are examined (Figures S2-S4). The results reveal inter-model discrepancies in the simulated ENSO-induced WNPAC pattern but show negligible changes in its position in response to future warming for any given model. The changes in ENSO-WNPAC correlation over the core region of WNPAC for each model, defined using a model-specific 20°×10° box, are consistent with the statistical results obtained using the fixed box approach (Figures 1d-k). This supports the robustness of our findings derived from the fixed-box WNPAC index.

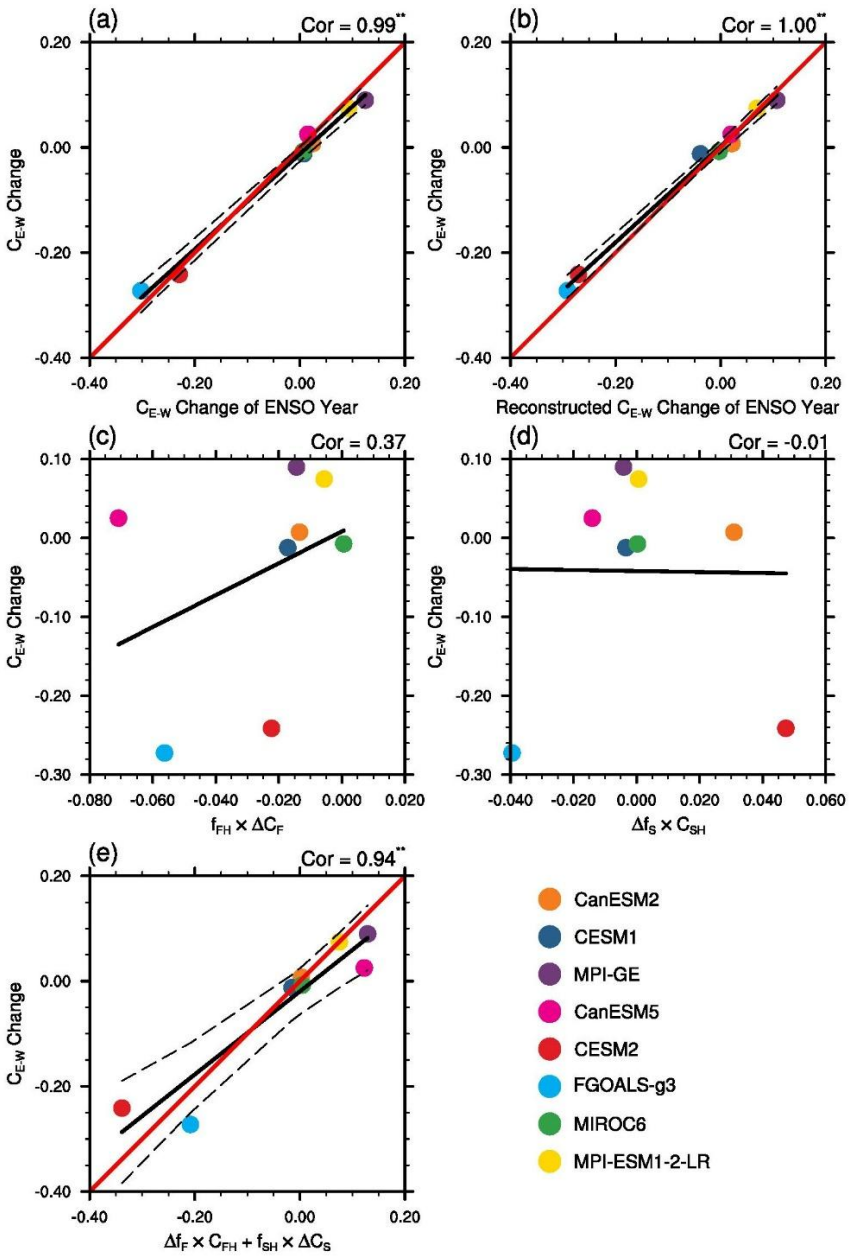

Figure S1. Model uncertainty of ENSO-WNPAC relationship changes related to different ENSO decaying regimes. (a) Inter-model relationship of $\Delta C_{E\text{-}W}$ between ENSO years and total years. (b) Same as (a) but for reconstructed $\Delta C_{E\text{-}W}$ following Equation (1). (c) and (d) Contributions of partial $\Delta C_{E\text{-}W}$ change of fast-decay ENSO (ΔC_F) and fraction change of slow-decay ENSO Δf_S, respectively, to total $\Delta C_{E\text{-}W}$. (e) Combined contributions of fraction change of fast-decay ENSO (Δf_F) and partial $\Delta C_{E\text{-}W}$ change of slow-decay ENSO (ΔC_S) to total $\Delta C_{E\text{-}W}$. Solid black lines are linear fitting across models and dashed lines show 95% ranges of the estimated mean $\Delta C_{E\text{-}W}$ based on the linear fitting. Red lines in (a), (b) and (c) denote that Y = X. Values on the top-right corner are correlation coefficients across models, with one asterisk (two asterisks) indicating significance at the 10% (5%) level under *t*-test.

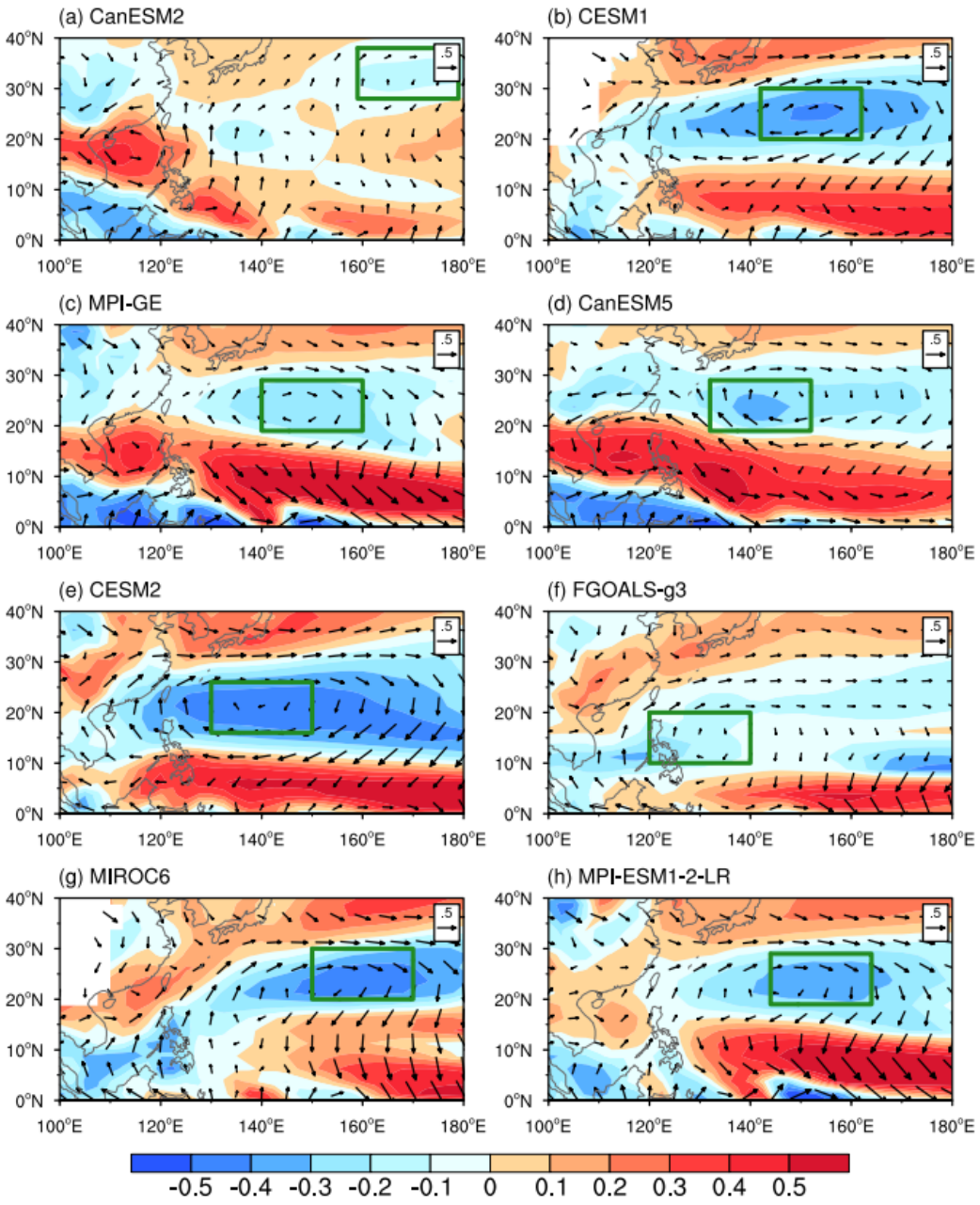

Figure S2. Patterns of correlation coefficient between D(-1)JF Nino3.4 index and JJA 850-hPa vorticity (shadings) and winds (vectors) during the historical period (1965-2005). Each panel represents the result for a specific model, with the core region of ENSO-induced WNPAC marked by a green box in a size of 20° longitude by 10° latitude.

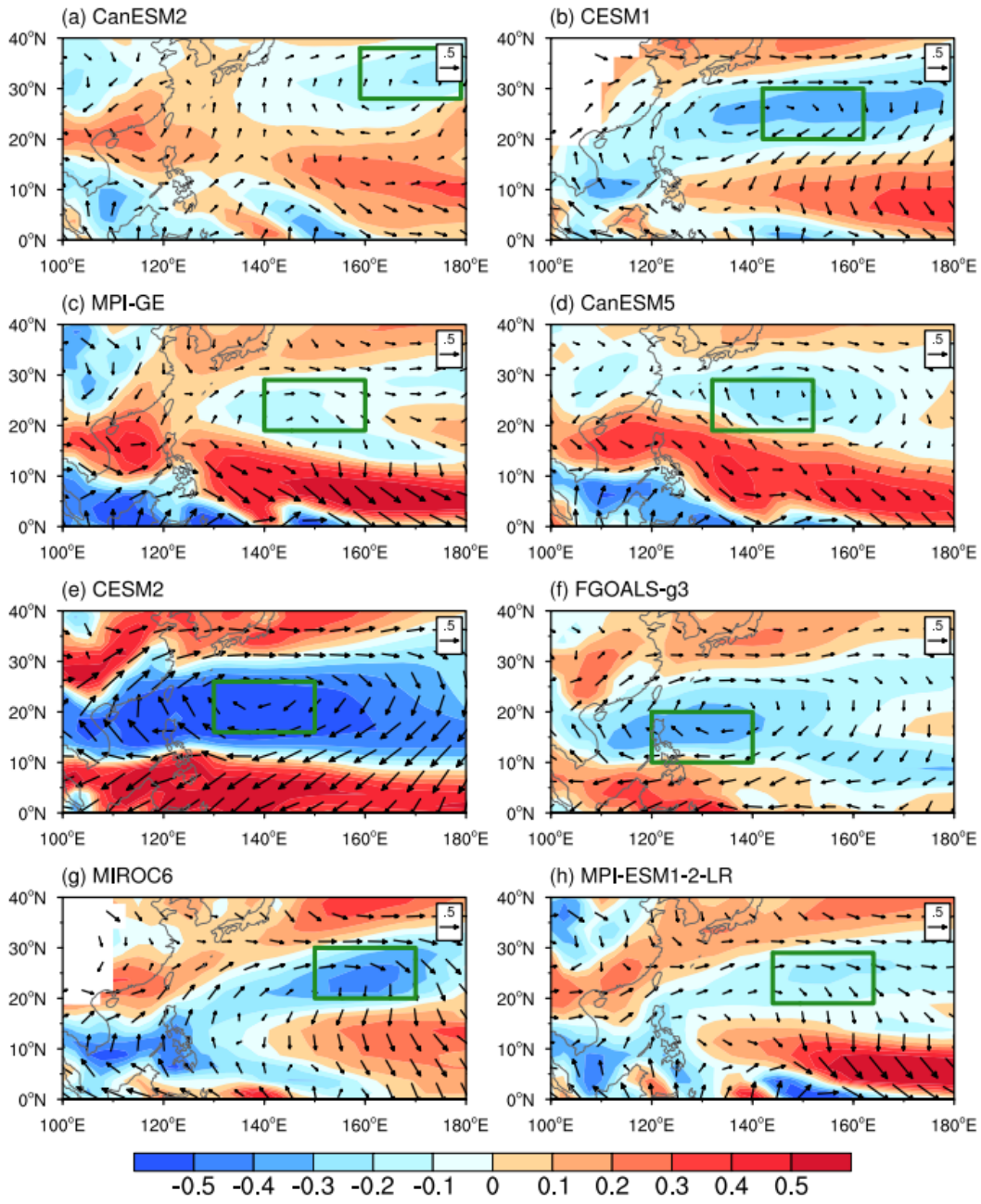

Figure S3. Same as Figure S2, but for the future period (2050-2099) under RCP8.5/SSP5-8.5 scenario.

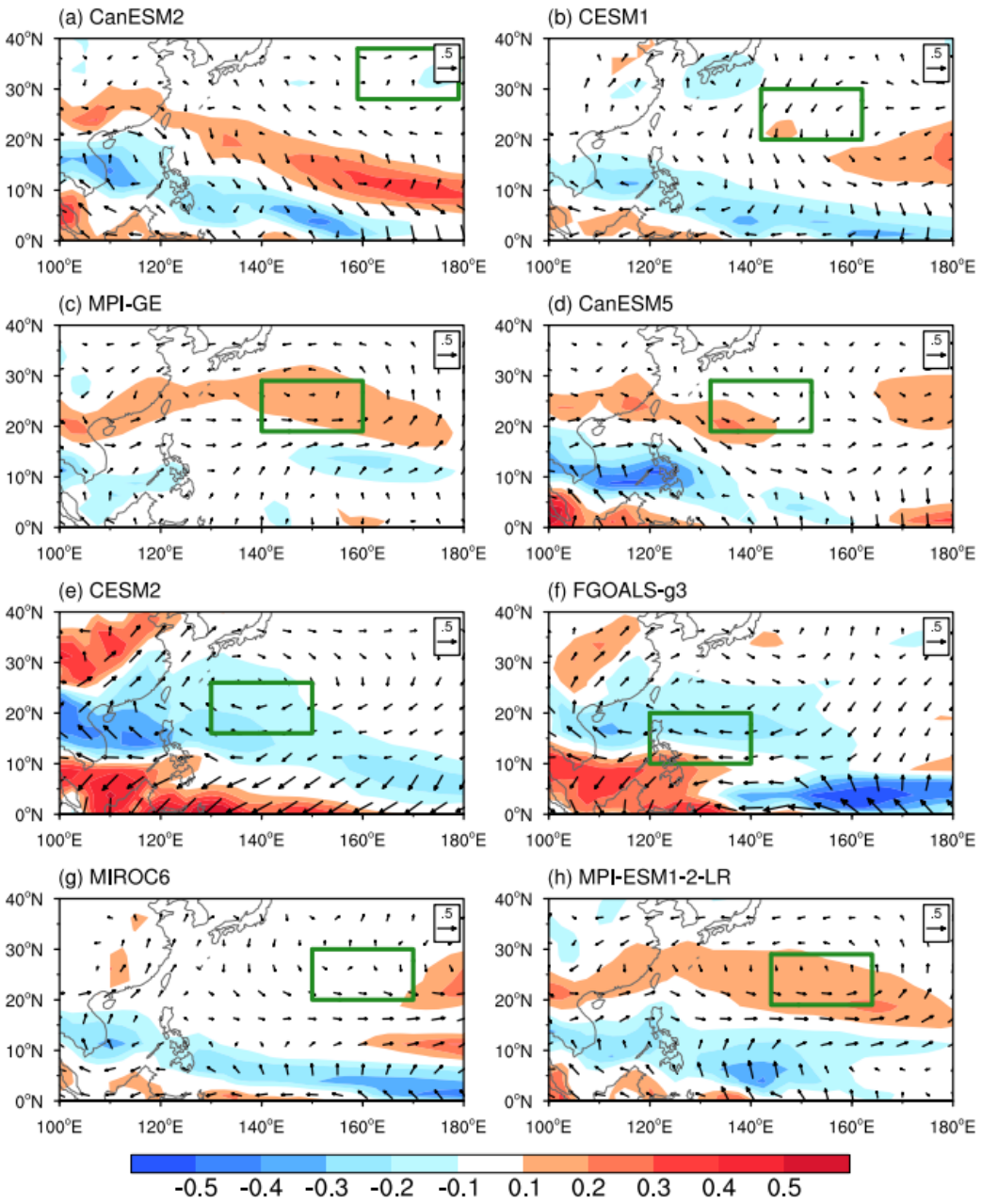

Figure S4. Same as Figure S2, but for difference between the future and historical periods.

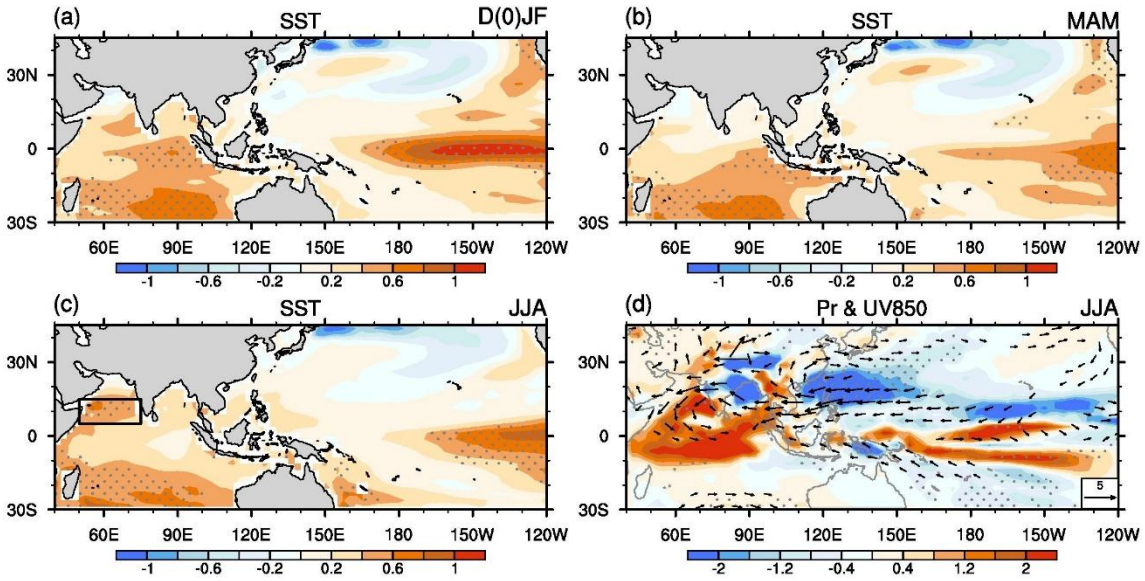

Figure S5. Impact of model spread in historical D(-1)JF ENSO intensity (slow-decay regime) on future change of ENSO-related anomalies over the WNP. (a-c) Inter-model regression coefficients (unit: K K^{-1}) of D(-1)JF Nino3.4-related SST anomalies under RCP8.5/SSP5-8.5 scenario onto historical D(-1)JF Nino3.4 intensity (σ_s) of slow-decay events. The black box (5-15°N, 50-75°E) in (c) is to define an index (unit: K) for JJA SST response in the Arabian Sea to D(-1)JF Nino3.4 under future scenario. (d) Inter-model regression coefficients of projected changes in D(-1)JF Nino3.4-related JJA precipitation (unit: mm day^{-1} K^{-1}) and 850-hPa wind anomalies (unit: m s^{-1} K^{-1}) onto the Arabian SST response index defined above in (c). Vectors with magnitudes larger than 1 are drawn. Dotted shadings mark the area with a statistical significance of the 10% level under *t*-test.

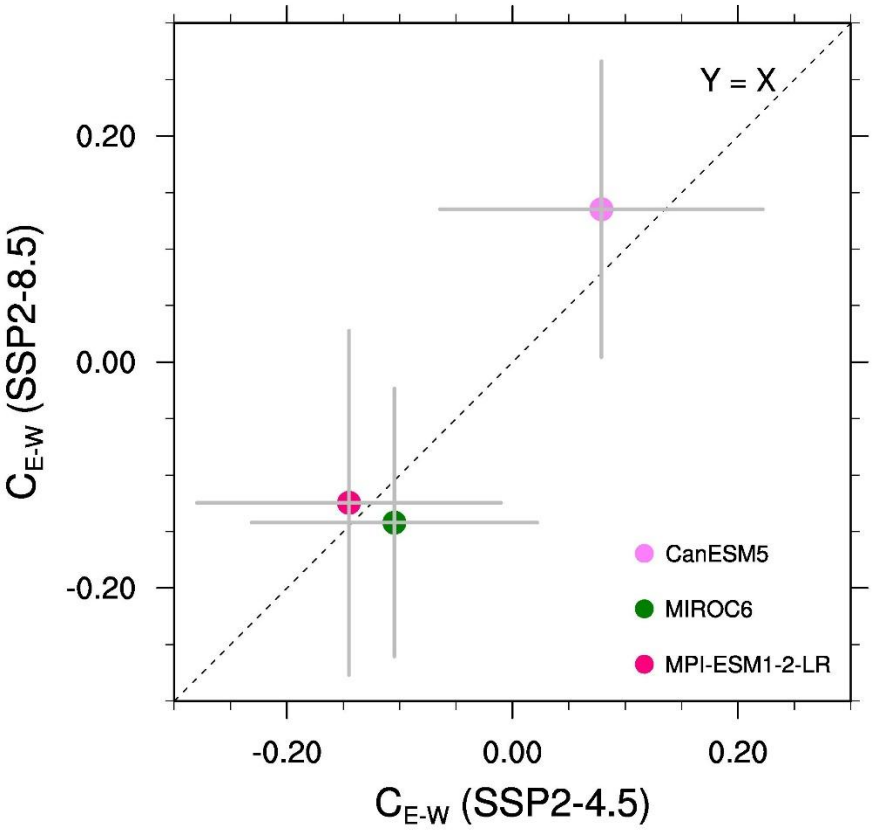

Figure S6. Comparison of the trans-seasonal ENSO-WNPAC correlation coefficients (C_{E-W}) between SSP2-4.5 and SSP5-8.5 during 2050-2099 in three CMIP6 models. The gray error bars represent the inter-member spreads (±1σ) caused by internal variability for SSP2-4.5 (X-axis) and SSP5-8.5 (Y-axis). The dashed diagonal line shows Y=X.

References

Bowman, K. W., Cressie, N., Qu, X., & Hall, A. (2018). A hierarchical statistical framework for emergent constraints: Application to snow-albedo feedback. *Geophysical Research Letters*, **45**, 13050–13059.

Chen, W., Lee, J.-Y., Ha, K.-J., Yun, K.-S., & Lu, R. (2016). Intensification of the western North Pacific anticyclone response to the short decaying El Niño event due to greenhouse warming. *Journal of Climate*, **29**, 3607–3627.

Chen, X., Zhou, T., Wu, P., Guo, Z., & Wang, M. (2020). Emergent constraints on future projections of the western North Pacific Subtropical High. *Nature Communications*, **11**, 2802.

Eyring, V., Bony, S., Meehl, G. A., Senior, C. A., Stevens, B., Stouffer, R. J., & Taylor, K. E. (2016). Overview of the Coupled Model Intercomparison Project Phase 6 (CMIP6) experimental design and organization. *Geoscientific Model Development*, **9**, 1937–1958.

Hu, S., Wang, L., Chen, X., Zhou, T., & Hsu, P.-C. (2024). Emergent constraints on future projections of Tibetan Plateau warming in winter. *Geophysical Research Letters*, **51**, e2024GL108728.

Kim, M., & Lee, E. (2022). Validation and comparison of climate reanalysis data in the East Asian monsoon region. *Atmosphere*, **13**, 1589.

Lin, P., Zhao, B., Wei, J., Liu, H., Zhang, W., Chen, X., et al. (2022). The Super-large ensemble experiments of CAS FGOALS-g3. *Advances in Atmospheric Sciences*, **39**, 1746–1765.

Maher, N., Milinski, S., Suarez-Gutierrez, L., Botzet, M., Dobrynin, M., Kornblueh, L., et al. (2019). The Max Planck Institute Grand Ensemble: Enabling the exploration of climate system variability. *Journal of Advances in Modeling Earth Systems*, **11**, 1–21.

O'Neil, B. C., Tebaldi, C., van Vuuren, D. P., Eyring, V., Friedlingstein, P., Hurtt, G., et al. (2016). The Scenario Model Intercomparison Project (ScenarioMIP) for CMIP6. *Geoscientific Model Development*, **9**, 3461–3482.

Rodgers, K. B., Lee, S.-S., Rosenbloom, N., Timmermann, A., Danabasoglu, G., Deser, C., et al. (2021). Ubiquity of human-induced changes in climate variability. *Earth System Dynamics*, **12**, 1393–1411.

Soci, C., Hersbach, H., Simmons, A., Poli, P., Bell, B., Berrisford, P., et al. (2024). The ERA5 global reanalysis from 1940 to 2022. *Quarterly Journal of the Royal Meteorological Society*, **150**, 4014–4048.

Taylor, K. E., Stouffer, R. J., & Meehl, G. A. (2012). An Overview of CMIP5 and the Experiment Design. *Bulletin of the American Meteorological Society*, **93**, 485–498.

Wu, M., Zhou, T., Chen, X., & Wu, B. (2020). Intermodel uncertainty in the projection of the Anomalous western North Pacific Anticyclone associated with El Niño under global warming. *Geophysical Research Letters*, **47**, e2019GL086139.

Wu, M., Zhou, T., & Chen, X. (2021). The source of uncertainty in projecting the anomalous western North Pacific anticyclone during El Niño–Decaying summers. *Journal of Climate*, **34**, 6603–6617.

Zhou, Z., Chen, X., Zhou, T., & Wu, B. (2024). Relationship between South Asian summer monsoon and ENSO primarily modulated by ENSO intensity based on two super large ensembles. *Climate Dynamics*, **62**, 10265–10279.